Mathematical Biosciences and Engineering

https://www.aimspress.com/journal/mbe

MBE, 21(3): 4370–4396.
DOI: 10.3934/mbe.2024193
Received: 31 August 2023
Revised: 04 January 2024
Accepted: 04 February 2024
Published: 27 February 2024

Research article

Modeling the impact of distancing measures on infectious disease spread: a case study of COVID-19 in the Moroccan population

Abdelkarim Lamghari[1,*], Dramane Sam Idris Kanté[1,2], Aissam Jebrane[2] and Abdelilah Hakim[1]

[1] LAMAI, Faculty of Sciences and Technics, Department of Mathematics, Cadi Ayyad University, Marrakesh 40140, Morocco

[2] Centrale Casablanca, Complex Systems and Interactions Research Center, Ville Verte, Bouskoura 27182, Morocco

* **Correspondence:** Email: abdelkarimsm@gmail.com.

Abstract: This paper explores the impact of various distancing measures on the spread of infectious diseases, focusing on the spread of COVID-19 in the Moroccan population as a case study. Contact matrices, generated through a social force model, capture population interactions within distinct activity locations and age groups. These matrices, tailored for each distancing scenario, have been incorporated into an SEIR model. The study models the region as a network of interconnected activity locations, enabling flexible analysis of the effects of different distancing measures within social contexts and between age groups. Additionally, the method assesses the influence of measures targeting potential superspreaders (i.e., agents with a very high contact rate) and explores the impact of inter-activity location flows, providing insights beyond scalar contact rates or survey-based contact matrices.
The results suggest that implementing intra-activity location distancing measures significantly reduces in the number of infected individuals relative to the act of imposing restrictions on individuals with a high contact rate in each activity location. The combination of both measures proves more advantageous. On a regional scale, characterized as a network of interconnected activity locations, restrictions on the movement of individuals with high contact rates was found to result in a 2% reduction, while intra-activity location-based distancing measures was found to achieve a 44% reduction. The combination of these two measures yielded a 48% reduction.

Keywords: COVID-19; contact matrices; inter-social context flows; Moroccan social contact patterns; distancing measures; social force model; SEIR model; infectious disease spread

1. Introduction

Being able to understand and predict the spread of infectious diseases is of paramount importance for public health and healthcare policy decision-making. The use of mathematical models to simulate disease dynamics has become a crucial tool for the assessment and mitigation of the impact of epidemics [1, 2]. However, a critical factor affecting the accuracy of these models lies in the proper characterization of interactions among individuals within the population. Social contact matrices constitute a tool to integrate these interactions into epidemiological models.

The first introduced compartmental models often assume homogeneity in interactions among individuals [3], which may not faithfully represent the complexity of real social interactions [4, 5]. Estimating social contact matrices has emerged as an approach to improve the predictive power of epidemiological models, especially in the context of the COVID-19 pandemic [6]. These matrices are constructed from data collected through questionnaires that inquire about the duration and nature of interactions among individuals in various social settings, such as schools, households, workplaces, and more. Statistical methods are then used to fill in data gaps [4]. These contact matrices are subsequently integrated into models to assess the impact of social distancing and containment measures. Restrictions are modeled by adjusting the coefficients of these contact matrices, where 0 represents complete confinement of the population in the relevant setting, and 1 indicates that there are no restrictions [7, 8]. However, this method does not allow one to capture the effect of social distancing [9].

There is a growing interest in estimating contact patterns by using the social force model (SFM) [10–12]. Recent studies on COVID-19 estimated contact frequencies in different settings [9, 13]. A recent approach using the SFM has introduced a spatio-temporal simulation of the spread of COVID-19 in different social contexts [14–16]. It allows one to capture context-specific interactions. This has paved the way for the estimation of contact matrices in various social contexts and under various demographic characteristics of the studied population (size and age distribution), interpersonal distances [17, 18] and desired walking speeds [19, 20].

These matrices integrate distancing measures between different age groups, which is essential for targeted vaccination strategies [21], isolating the most exposed age groups, or managing individuals with a high potential for transmission.

In this study, we propose a reevaluation of distancing measures by using the new contact matrices generated by the SFM. We address three key aspects:

i) The integration of the new contact matrices into an SEIR model to study disease propagation within populations in various activity settings and compare the results with those obtained from traditional matrices.
ii) The evaluation of the impact of social distancing as considered in the new contact matrices and a comparison with the results of restrictions applied in other models.
iii) The explicit consideration of flows between different activity settings by simulating a region as a collection of interacting social contexts connected through these flows.

The structure of this article is as follows. In Section 2, we present the models used for each case, starting with a single social context and then extending the analysis to all social contexts that comprise the total population. Section 3 presents the results and discussion.

2. Materials and methods

2.1. Estimation of contact matrices via a modified SFM

First, we will briefly summarize the method for contact matrix estimation. This method entails modeling interactions within populations from various social contexts by using an SFM, and as based on demographic and sociocultural data. Figure 1 illustrates the process, and for more details, we refer the reader to Appendix A.1.

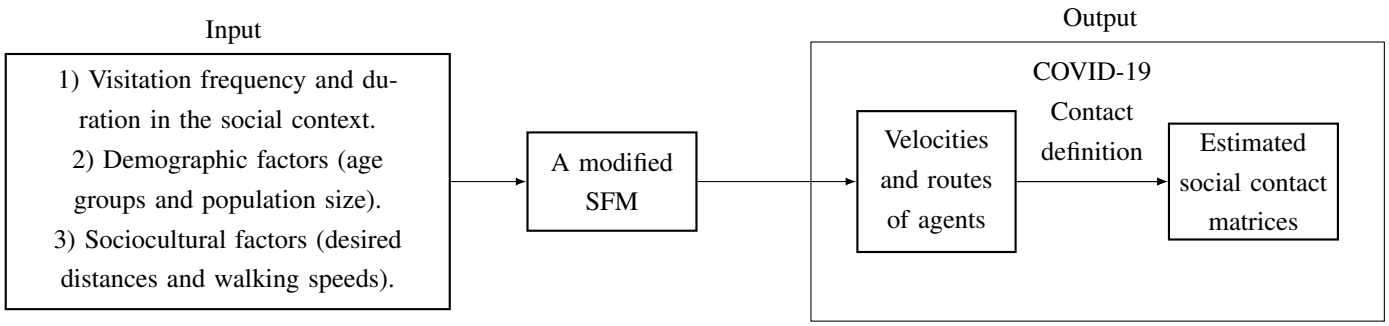

Figure 1. Illustration of the method to estimate COVID-19-related contact matrices in a social context: First, the geometry of the social context and the demographic characteristics of the population are considered. Then, the duration and frequency of visits, as well as data on the desired walking speeds and distances, are integrated based on the modeled scenario,regardless of whether it involves normal interactions or restrictions. These data are subsequently used in a modified version of the SFM to simulate the movements of the population. Ultimately, by applying the appropriate definition of COVID-19-related contact, contact matrices by age group are generated.

2.2. A contact-structured SEIR model for disease spread in asingle social context

The dynamics of disease transmission can vary depending on the social context in which it occurs and the age distribution of the population under consideration. We employ an age-structured SEIR model in a social context [5, 8]. A contact matrix C is used to determine the contact rates between different age groups. The elements of the matrix C_{ij} represent the rates of contact between individuals belonging to age groups $i, j = 1...M, M = 16$. We shall describe the evolution of populations of susceptible S_i, exposed E_i, infected I_i, and recovered R_i individuals for each age group i by using the following system:

$$\begin{cases} \frac{dS_i}{dt} = -\lambda_i(t)S_i \\ \frac{dE_i}{dt} = \lambda_i(t)S_i - \gamma_E E_i \\ \frac{dI_i}{dt} = \gamma_E E_i - \gamma_I I_i - \alpha_i I_i \\ \frac{dR_i}{dt} = \gamma_I I_i \end{cases}, \tag{2.1}$$

where $\lambda_i(t) = \beta \sum_{j=1}^{M} \left(C_{ij} \frac{I_j}{N_j} \right)$ is the disease transmission rate; β is the probability of infection upon contact. γ_E is the average infectious period, while γ_I denotes the recovery rate, and α_i represents the mortality rate for age group i. To estimate the COVID-19 mortality rate within a specific age group, we chose to rely on the infection-to-fatality ratio (IFR) described in [22, 23], as well as the infection prevalence data from [24].

It is important to note that our use of the SEIR model serves as an illustrative example. We can utilize alternative age-structured compartmental models that integrate contact matrices, or even more advanced models specifically designed for COVID-19 [25]. Nevertheless, our main emphasis remains on the contact matrices and the unique benefits of computing them by using the SFM, as demonstrated in the results section, rather than relying on questionnaires.

2.3. Extending the SEIR model to a connected network of social contexts

We conceptualize a global region as a network of interlinked social contexts, encompassing workplaces, schools, households, and shopping centers, among others. Our primary attention is directed toward four central activity hubs: schools, residences, workplaces, and shopping centers. We elucidate the virus transmission dynamics within each social context by employing the SEIR model. The interrelations between these contexts are depicted by using a flow matrix F, with F_{AB} signifying the population migration rate from social context A to social context B. This rate is 25% for all places. The visual representation below provides an overview of the global SEIR model applied to these interconnected activity locations, as illustrated in Figure 2.

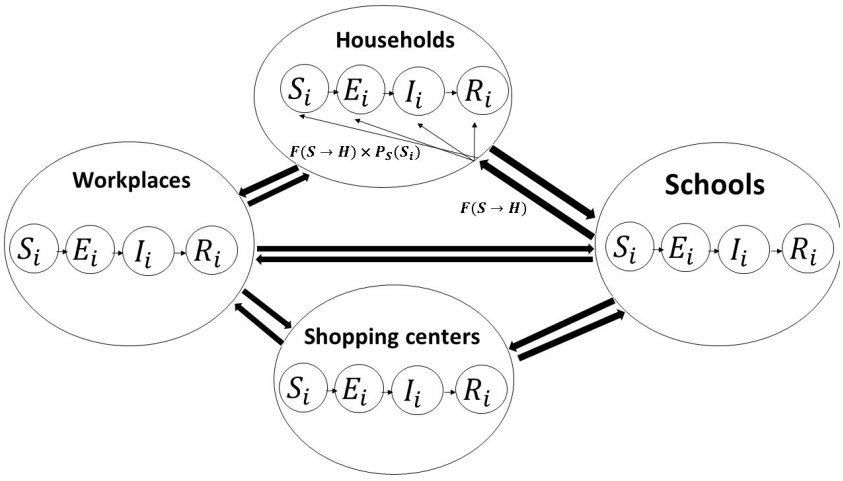

Figure 2. An overview of the global SEIR model for interconnected social contexts: $F(S \to H)$ represents the percentage of the school population moving towards households. $P_S(S_i)$ denotes the percentage of the susceptible population in age group i within schools, and $F(S \to H) \times P_S(S_i)$ is the rate of the susceptible population in age group i moving from schools to households.

3. Numerical results

3.1. Simulations settings

The chosen case study is the spread of COVID-19 in Morocco. Demographic features of the Moroccans' age distribution were estimated in [26,27]. The death rate was sampled by age group [28,29]. The parameters of the SEIR model are summarized in Tables 1 and 2. We utilize the decision factor I to assess the effectiveness of a restriction measure.

$$I = 100 \times \left(1 - \frac{I^{\text{cuml}}_{\text{matrix C}}}{I^{\text{cuml}}_{\text{Normal matrix}}}\right), \tag{3.1}$$

where $I^{\text{cuml}}_{\text{matrix C}}$ is the cumulative number of infected individuals when we apply a measure, and $I^{\text{cuml}}_{\text{Normal matrix}}$ is the cumulative number of infected individuals in the absence of measures.

Table 1. Model parameters.

Definition	Symbol	Value	Reference
Transmission probability per contact	β	0.0962	[30]
Daily contact rate	C_{ij}	Age-dependent	[5, 14]
Population size	N_i	36.91×10^7 by age group	[26, 27]
Average infectious period	γ_E	$\frac{1}{14}$	[31]
Recovery rate	γ_I	6.19×10^{-4}	[30]
Mortality rate	α_i	Age-dependent	[22, 32]

Table 2. Mortality rate α_i and demography by age group [26–29].

Age bracket	**Mortality rate** (%)	**Demography** (%)
0–4	0.005	9
5–9	0.0009	9.4
10–14	0.001	8.6
15–19	0.0045	8.1
20–24	0.009	7.8
25–29	0.015	8.2
30–34	0.035	7.8
35–39	0.06	7.6
40–44	0.07	6.5
45–49	0.085	5.7
50–54	0.3	5.3
55–59	0.55	4.9
60–64	0.65	4.3
65–69	1	3.3
70–74	2	1.9
75–79	4	1.5

Detailed demographic distributions by age bracket within various activity locations can be found in Appendix A.6.

3.2. Infection dynamics within a single social context

3.2.1. Epidemiological curves: contact matrices derived from the SFM in a Moroccan shopping center

In this section, we assess the impact of social distancing measures on disease spread in a shopping center with 2000 people. Contact matrices were estimated by using the SFM. The figures below illustrate contact patterns in normal and social distancing scenarios. The contact matrix shown in Figure 3(A) was constructed by considering the population's typical movements and interactions in a Moroccan shopping center, taking into account sociocultural factors such as desired distance and walking speed, as described in [14, 33]. The desired distance corresponds to a personal social distancing range, specifically ranging from 0.4 meters to 1.2 meters. In contrast, the contact matrix shown in Figure 3(B) represents distancing restrictions among individuals, replacing the personal distance with a public distance of 3 to 4 meters. For a comprehensive description of social distances, refer to Table 6 in Appendix A.5.

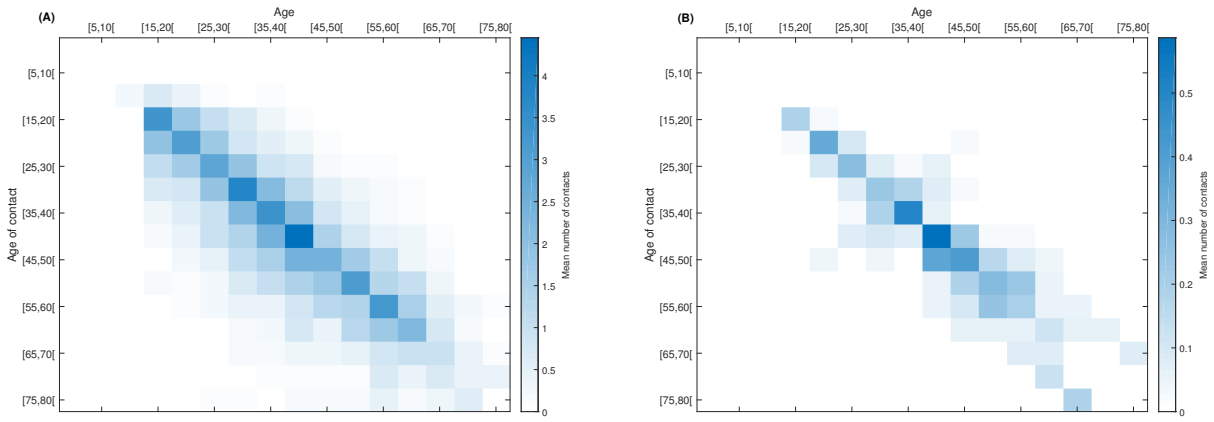

Figure 3. Visualization of SFM-based contact matrices for a population in a Moroccan shopping center: A) without Distancing, and B) with Distancing.

In Figure 4, the SEIR model was applied by using the contact matrices computed by using the SFM. The implementation of stringent social distancing measures in the shopping center resulted in a 33.3% reduction in the peak, decreasing from 600 to 200 infectious agents. In terms of the cumulative number of infections, we can see a reduction of 60%, going from 42850 individuals in the scenario without distancing to 17160 individuals in the scenario with distancing.

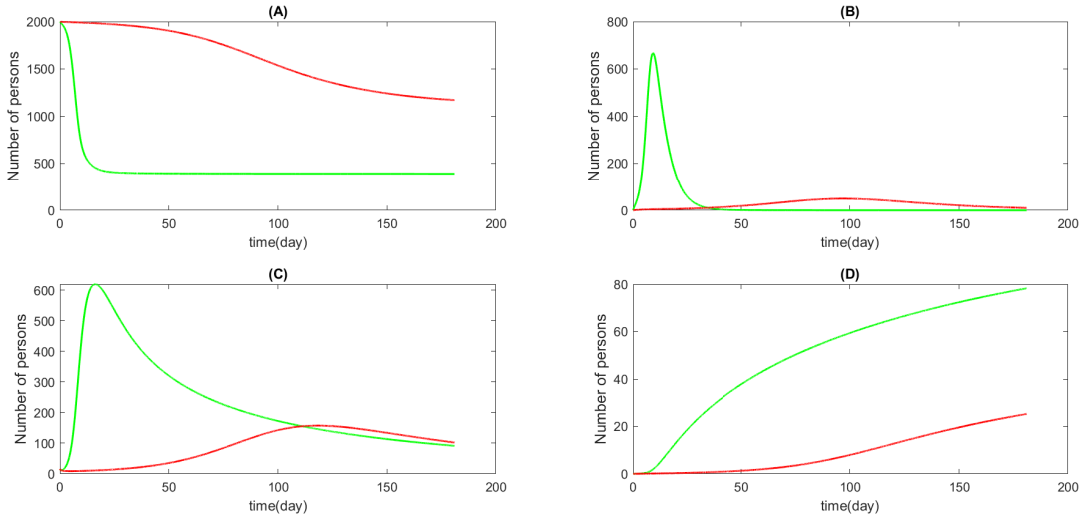

Figure 4. Comparison of epidemiological curves associated with SFM-based contact matrices, with distancing (red curve) and without distancing (green curve) in a shopping center in Morocco. (A) the susceptible population, (B) the exposed population, (C) the infectious population, and (D) recovered individuals.

We also chose to investigate the impact of restricting interactions among age groups with the highest contact rates (35 to 39 years, 40 to 44 years, and 45 to 49 years) and the others. Figure 5 compares the effects of implementing social distancing measures, imposing restrictions only on individuals with high contact rates, and combining both restrictions. It is evident that social distancing measures are much more effective than targeting specific age groups with very high contact rates. The epidemiological curves for various social contexts under social distancing measures, using our estimated contact matrices, were derived as presented in Appendix A.3.

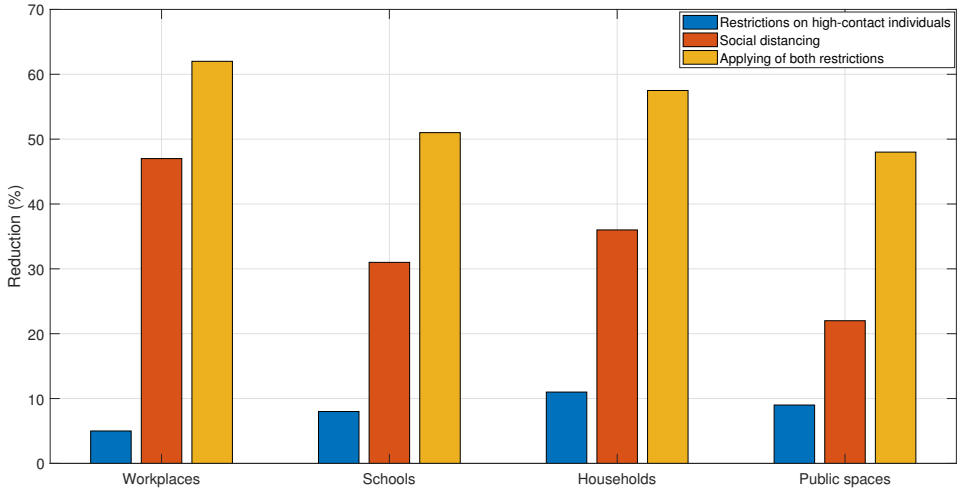

Figure 5. Reduction rates for infectious individuals in various social contexts under different restrictions.

3.2.2. Comparison of epidemiological curves derived from SFM-based contact matrices and survey-based contact matrices

We obtained contact matrices for Morocco from a study that projected contact matrices based on questionnaires for 152 countries [5], as indicated in Appendix A.2, Figure 11. We also used contact matrices based on the SFM. Subsequently, we compared the epidemiological curves derived from the two sets of matrices within different social contexts. Figure 6 displays the curves in the case of schools, while the curves for other social contexts are provided in Appendix A.4. The cumulative number of infectious individuals was 1.3×10^9 for the estimated matrix and 1.38×10^9 for the survey-based contact matrix. These figures indicate a close alignment between the results obtained from the two sources. A comparison of the infection dynamics for other settings, as determined by using SFM-based and survey-based contact matrices is presented in Appendix A.4.

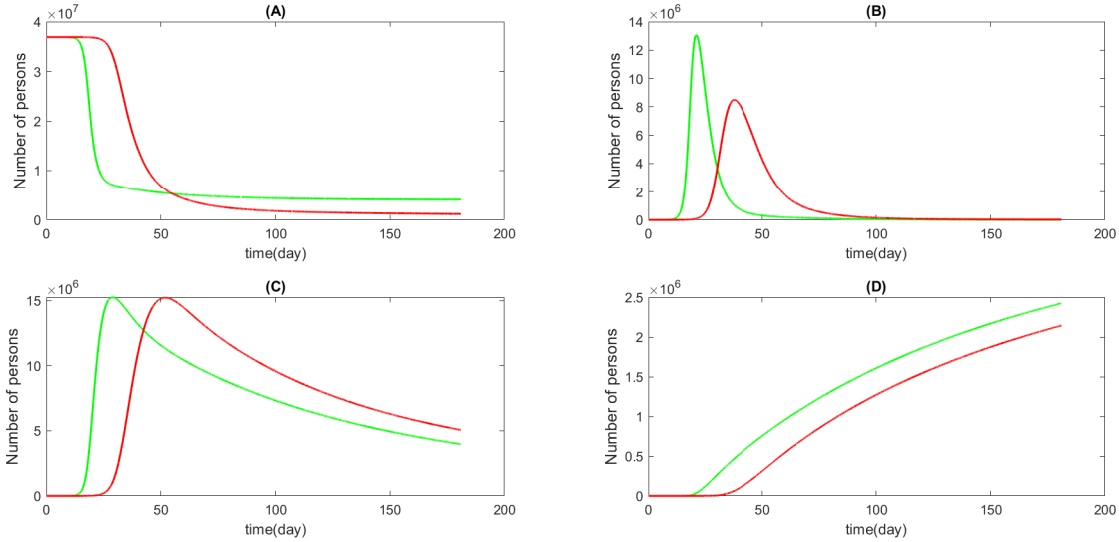

Figure 6. SFM-based contact matrix (green curve) versus survey-based contact matrix (red curve) for schools: (A) evolution of susceptible individuals; (B) evolution of exposed individuals; (C) evolution of infectious individuals; (D) evolution of recovered individuals.

3.3. Infection dynamics in connected social contexts with integration of social distancing

This subsection details the examination of the spread of infectious diseases in connected social contexts by incorporating social distancing measures.

First, let us recall the traditional method for the integration of social contact matrices. Let C_{ij} represent the total average number of contacts between an individual in age group i and individuals in age group j across various social contexts. In the context of contact matrices based on questionnaires, the incorporation of distancing measures into epidemiological models is expressed by the following formula:

$$C_{ij} = C_{ij}^H + \alpha C_{ij}^S + \beta C_{ij}^W + \gamma C_{ij}^O \quad [8]\,, \tag{3.2}$$

where C_{ij}^H, C_{ij}^S, C_{ij}^W, and C_{ij}^O denote the contact numbers in households (residential areas), workplaces,

schools, and other locations (public spaces and shopping centers); α, β, γ are control parameters with values between 0 and 1 that are forced on non-household contacts to account for social distancing. This approach supposes homogeneity in compliance with social distancing. However, some studies estimate that adherence to distancing may depend on age and sociocultural factors [34, 35]. The SFM-based contact matrices estimated in a social distancing scenario account for this heterogeneity through demographics and interpersonal distances. For the first simulations described in this section, we applied $\alpha, \beta, \gamma = 1$ in both the normal and social distancing scenarios. The incorporation of social distancing measures into the SFM-based contact matrices significantly reduced the total cumulative infectious count from 1.533×10^{10} to 4.48×10^{9} (Figure 7). We also integrated these contact patterns into the compartmental model, as shown in Figure 7. Results show that social distancing resulted in a reduction of 43% (Figures 8, 9). This reduction is less than 50% and might need to be combined with other intervention measures.

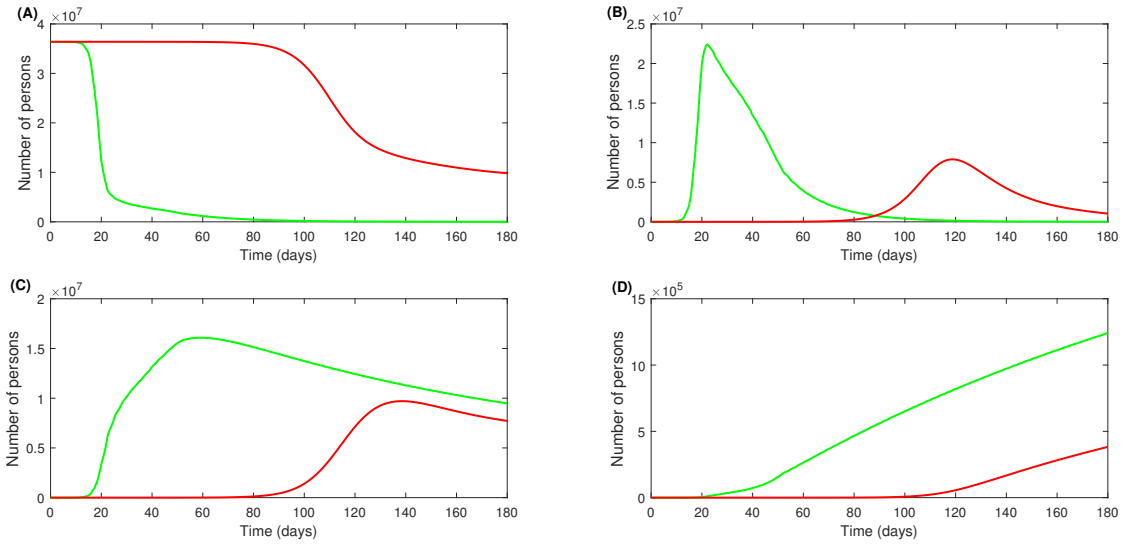

Figure 7. Comparison of epidemiological curves in a scenario with (red curve) and without (green curve) social distancing. Contact matrices were calculated by using the SFM. $C_{ij} = C_{ij}^{H} + C_{ij}^{S} + C_{ij}^{W} + C_{ij}^{O}$, with no flow considered between social contexts. (A): evolution of susceptible individuals. (B): evolution of exposed individuals. (C): evolution of infectious individuals; (D): evolution of recovered individuals.

Then, we chose to study the effect of restrictions on the movement of age groups with high contact rates. These age groups could be considered as potential superspreaders [13]. In each social context, the age groups with the highest contact rates are identified, and then the displacement of this age group from the residential area is cut off. For example, individuals aged 20–24 were found to have the highest contact rate in residential areas and shopping centers. The flow of movement of this age group toward shopping centers is also cut off; however, they were able to move to other contexts.The results are presented in Table 3.

Results in Figure 9 show that restricting specific age group movements is not an efficient intervention measure. These results are consistent with the idea that group-targeted restriction measures are not as efficient as when a whole community is restricted from movement [36, 37].

3.4. Combination of social distancing and global movement restrictions

Here we describe the results of integrating social distancing contact matrices into the SEIR model with interconnected social contexts. This measure has been combined with restrictions on movement. We study the effect of cutting off the flux of displacement towards each social context. The results show that closing schools is more effective with a reduction of 92%, followed by public places at 75.94%, and shopping centers at 66.92%, Figure 10. Another area of research also associates the combination of school closure and other measures with a reduction in COVID-19 cases [38]. Overall in this study combining social distancing with global restriction of movement from households to other social contexts achieved the greatest reduction in the number of infections.

Table 3. Results of the age groups found by combining the contact matrix of households with other contact matrices of the remaining places of activity.

Places of activity	Workplaces	Schools
Age groups	20-24 ; 24-29 ; 30-34 ; 35-39 ; 40-44 ; 45-49 ; 50-54 ; 55-59 ; 60-64	10-14 ; 15-19 ; 20-29 ; 30-34 ; 35-39 ; 40-44 ; 55-59
Places of activity	Public spaces	Shopping centers
Age groups	20-24 ; 24-29 ; 30-34 ; 35-39 ; 40-44 ; 45-49 ; 50-54 ; 55-59 ; 60-64 ; 65-69 ; 70-74	20-24 ; 24-29 ; 30-34 ; 35-39 ; 40-44 ; 45-49 ; 50-54 ; 55-59 ; 60-64 ; 65-69

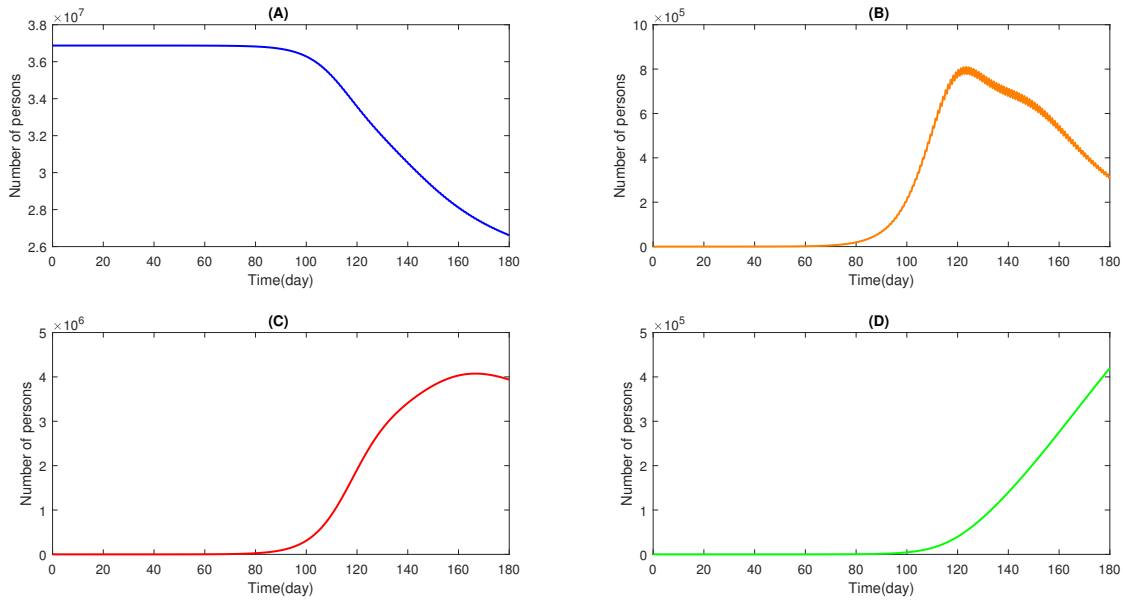

Figure 8. Epidemiological curve results based on confinement by age group (superspreaders) and social distancing restriction with flux. (A) The evolution of susceptible individuals. (B) The evolution of exposed individuals. (C) The evolution of infectious individuals. (D) The evolution of recovered individuals.

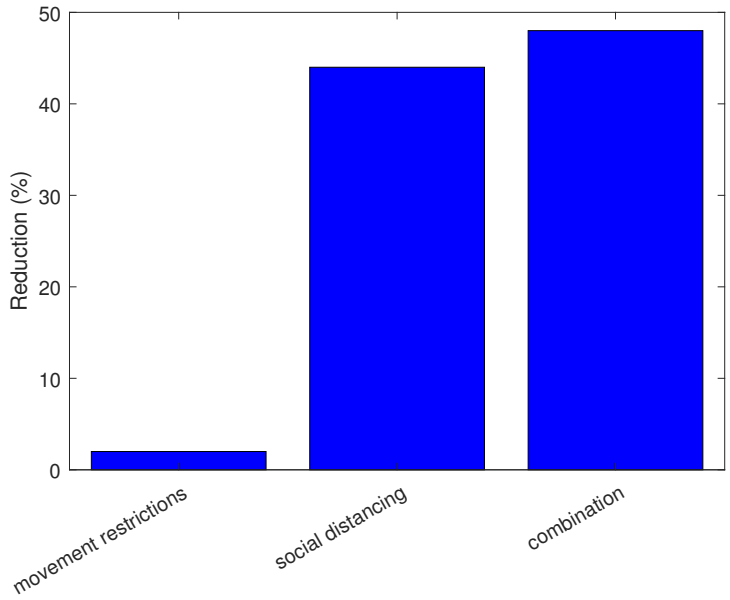

Figure 9. Global reduction rate associated with superspreader restrictions and Social distancing with flux.

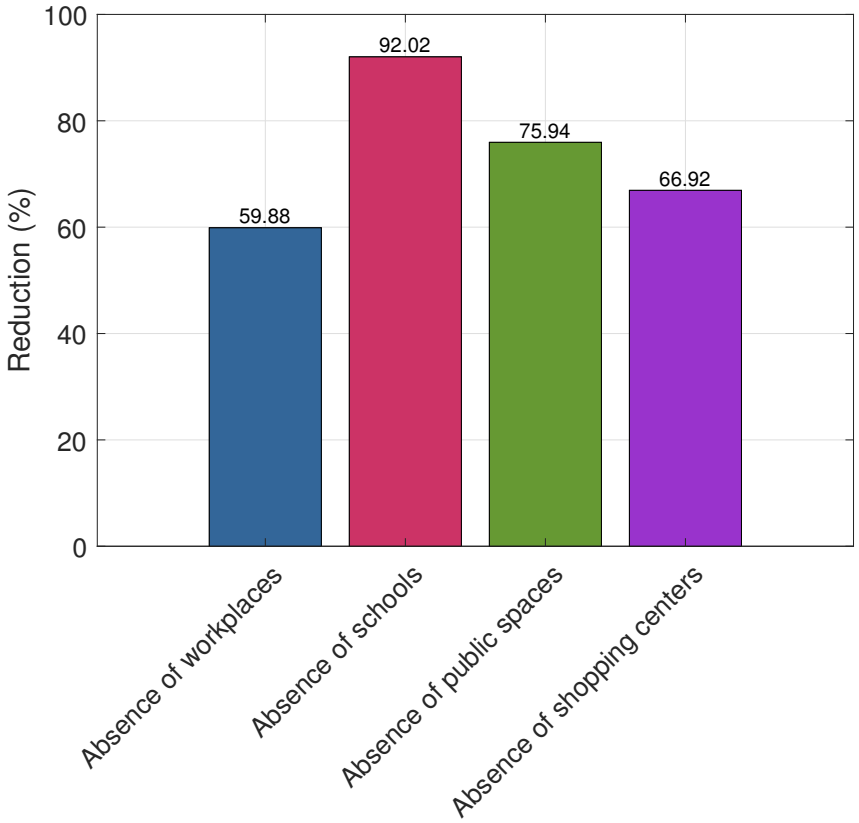

Figure 10. Reduction rate associated with global movement restrictions with flux.

4. Conlusions

Non-pharmaceutical measures allow one to delay the peak of an epidemic, which allows governments to anticipate and prevent their socio-economic impacts. Mathematical models provide tools to test these measures by simulating artificial populations. The data integrated into these models are generally estimated based on surveys. These questionnaires estimate contact patterns between individuals which depend on the demographics and sociocultural characteristics of the studied population. In this study we integrated contact patterns that were estimated by using the SFM. This method allows us to simulate interactions between individuals in a synthetic population representing the Moroccan population. Simulations take into account demographic and sociocultural characteristics such as the interpersonal distances between individuals. Contact patterns estimated under the conditions of a social distancing scenario take into account the disparity observed in compliance with this measure. Furthermore, we have used an SEIR model where social contexts are interconnected. This approach allows one to model movements between different contexts.

First, we studied the impact of social distancing in a single social context. The results show a 44% reduction in the number of cumulative infections. Simulations showed that restricting high contact rates individuals interactions was not impactfull.

Next, we simulated the infection dynamics by considering social contexts that are interconnected. with this configuration we studied the effectiveness of social distancing, restricting the movements of age groups with high contact rates, the combination of these last two, and the combination of social distancing and the closure of each social context. The results show that restricting the movement of specific age groups who may be potential superspreaders is less effective than social distancing. Other studies have shown that measures targeting specific age groups are not very effective [36, 37]. Social distancing reduced the number of infections by 44%. The effectiveness of social distancing has been discussed in previous works. Some scholars have presumed its ineffectiveness to be due to the heterogeneity observed in adherence to this measure [34]. Other studies support the effectiveness of social distancing, especially when combined with other intervention measures [39, 40]. In our study a combination of social distancing with other measures appears to be key to mitigating COVID-19 propagation. Its combination with global movement restrictions that were independent of age had the greatest impact. Furthermore, simulations revealed that its combination with school closures is more effective.

In this work, we developed an approach that allows the integration of contact matrices derived from SFMs. Estimated contact matrices can be an alternative to questionnaire-based methods. The approach used is a compartmental model in which social contexts are interconnected. We believe that this work contributes to the field because it yielded ideas that would improve the quality of predictions in the context of preventing the spread of emerging infectious diseases.

Appendix A.

Appendix A.1. Computation of contact matrices

Contact matrices were estimated by using a social force model (SFM). The SFM allows one to simulate interactions within a community as well as interactions with the environment. The model was introduced by Helbing and Molnar [10]. It has been modified to account for interpersonal distances between agents. The equation is as follows:

$$m_i \frac{d\mathbf{v}_i}{dt} = \mathbf{f}_i^{self} + \mathbf{f}_i^{soc} + \mathbf{f}_i^{obs}, \tag{4.1}$$

where m_i is the mass of an agent that influences its response to external forces and contributes to its realistic behavior simulation, $\mathbf{v}_i$ is the agent's velocity, which determines the speed at which the agent moves in the SFM, and $\mathbf{f}_i^{self}$ represents the self-driven force that allows the agent to tailor their speed to a desired velocity. $\mathbf{f}_i^{soc}$ is the social repulsive force that integrates each agent's personal space. $\mathbf{f}_i^{obs}$ is a repulsive force that keeps agents from colliding with walls and obstacles. Further details on the model are provided in [10, 11]. To compute the contact matrices, sociocultural and demographic data stratified by age group were collected on the basis of agent behavior in different social contexts. These data include interpersonal distances [18], which define agents' personal spaces, desired walking velocities [41], weights [42–45], the prevalence of each age group in each social context [46–51], and other parameters of the SFM.

We have taken into consideration the safety distance for respiratory infectious diseases to determine contact between two pedestrians. We then considered the duration of exposure required to breathe in an infectious dose while staying inside the specified safety zone. We have defined contact as an interaction in which two agents remain within 1.8 m of each other for 30 seconds [52, 55]. Any additional interaction between two individuals is not counted after their initial encounter [57]. A matrix C_{ij}, which is the total number of encounters between each age group, is the result of our simulations. Next, we constructed a matrix m_{ij} that estimates the mean number of interactions between a person in age group i and agents in age group j such that $C_{ij} = m_{ij} \times n_i = m_{ji} \times n_j = C_{ji}$, where n_i and n_j are the respective age groups. For each social context, we estimated the contact matrices throughout the activity. We took into account eight hours of activity at schools [53,60], five hours in homes [56], eleven hours in malls [63], and lastly eight hours and sixteen hours, respectively, at workplaces and other locations [54]. In our simulations, each agent spent an average of 135 minutes [58] at the shopping center during the 11-hour opening period.To account for social distancing each agent's interpersonal distance was set to 2 m in each social context.

Appendix A.2. Survey-based contact matrices

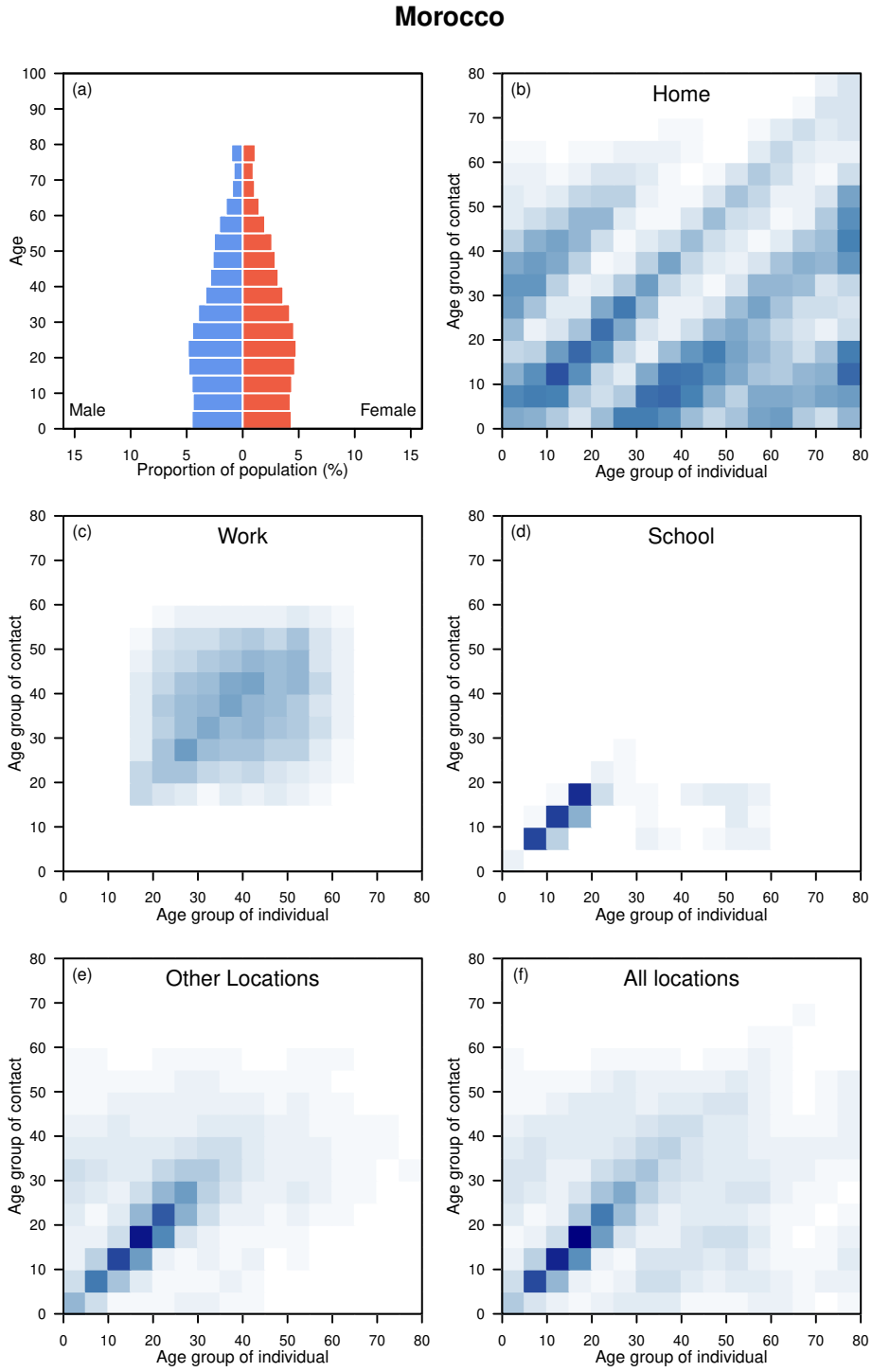

Figure 11. Illustration of survey-based contact matrices for data from Morocco. The color intensity of each cell represents the mean number of contacts between an individual in one age group and individuals in another age group across various social contexts. Figure adapted from [5].

Appendix A.3. Determining the infections dynamics in a social context with social distancing integration by using our estimated contact matrices

We constructed epidemiological curves in various social contexts (households, workplaces, schools, and public spaces) that incorporate social distancing measures by utilizing our estimated contact matrices.

Appendix A.3.1. Influence of social distancing on household infection transmission

In Figure 12, we present a comparison of the epidemiological curves for normal and social distancing contact within households. The figure illustrates that social distancing reduces the number of susceptible, exposed, and infectious individuals, while increasing the number of recovered individuals. As shown in the figure, social distancing also delays and lowers the infectious curve peak.

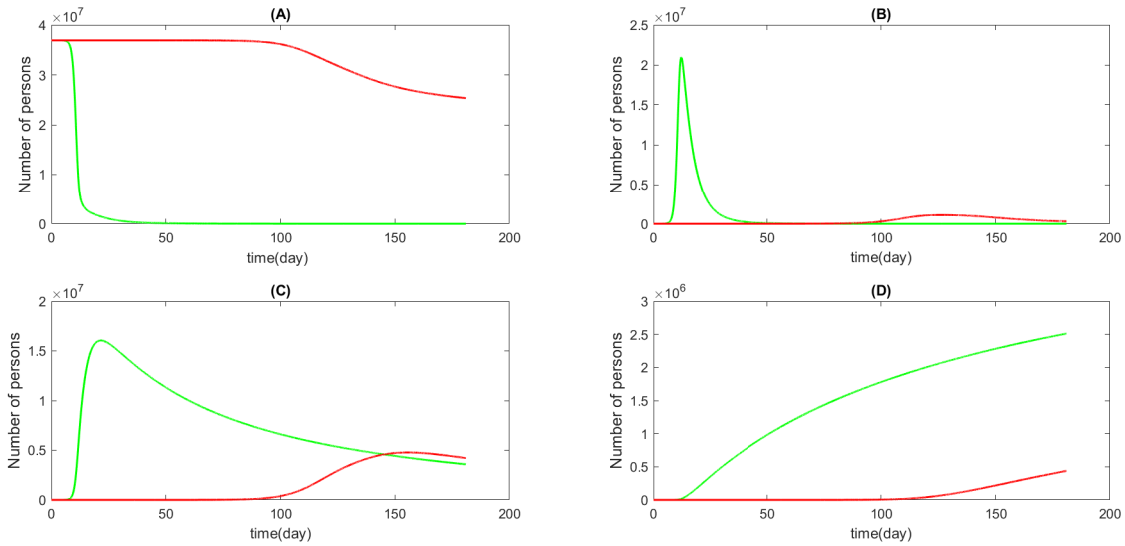

Figure 12. Normal contact matrix (green curve) versus social contact matrix (red curve) within households. (A): evolution of susceptible individuals. (B) : evolution of exposed individuals. (C): evolution of infectious individuals. (D): evolution of recovered individuals.

Appendix A.3.2. Influence of social distancing on workplace infection transmission

In Figure 13, COVID-19 epidemiological curves with and without social distancing measures are compared. As compared to the green curve without social distancing, the red curve showed greater protection for the population, lower potential for new infections, a reduction in the epidemic peak, and a reduction in mortality.

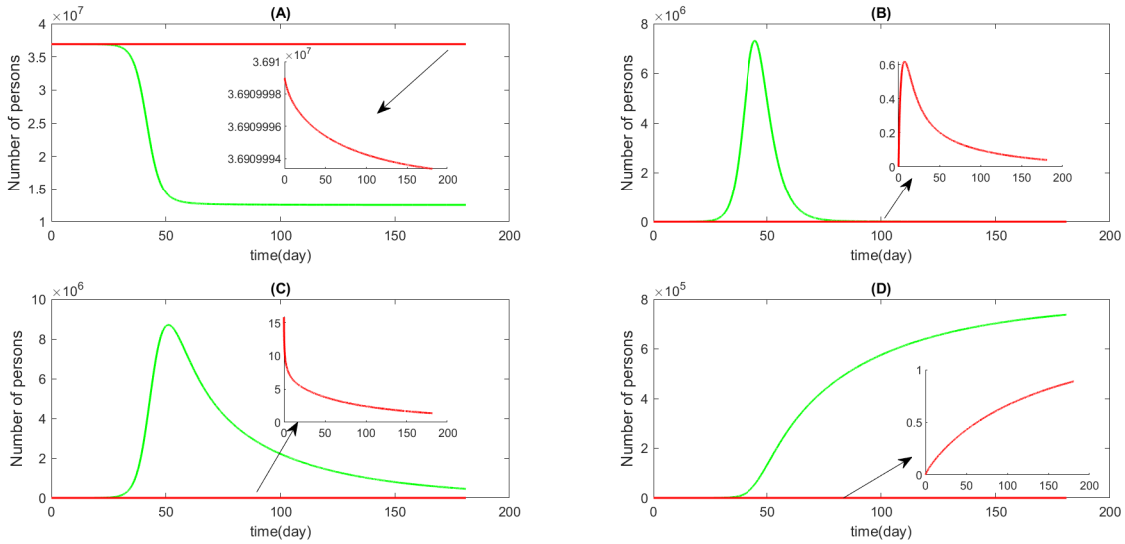

Figure 13. Normal contact matrix (green curve) versus social contact matrix (red curve) within workplaces. (A): evolution of susceptible individuals. (B): evolution of exposed individuals. (C): evolution of infectious individuals. (D): evolution of recovered individuals.

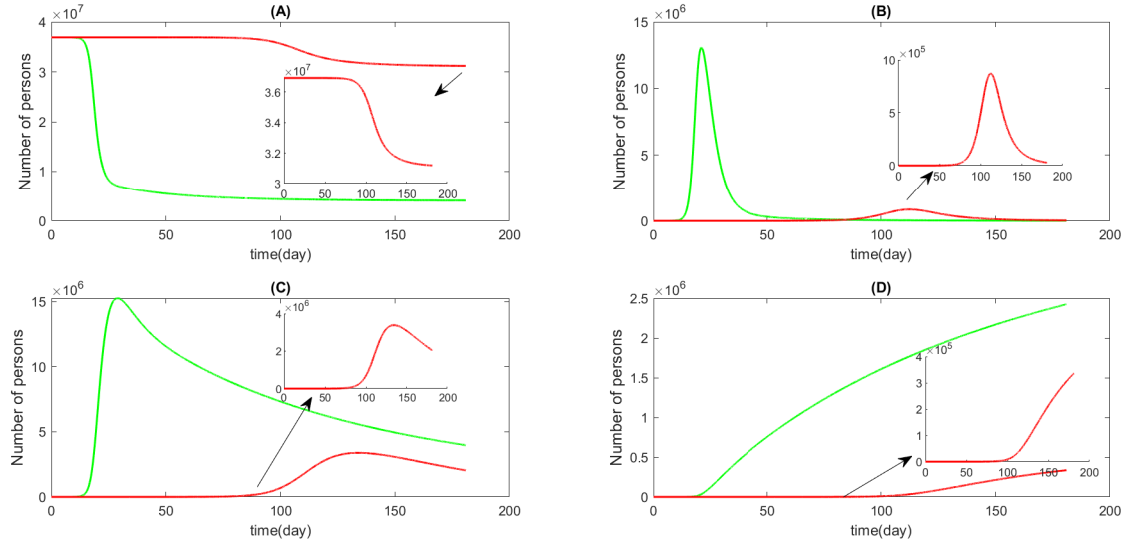

Figure 14. Normal contact matrix (green curve) versus social contact matrix (red curve) within schools. (A): evolution of susceptible individuals. (B): evolution of exposed individuals. (C): evolution of infectious individuals. (D): evolution of recovered individuals.

Appendix A.3.3. Influence of social distancing on school infection transmission

In Figure 14, the epidemiological curves for schools are presented for two contact matrices: a normal contact matrix (green) and a social distancing matrix (red). As compared to the no-distancing scenario, social distancing lowers the number of susceptible, exposed, infected, and recovered people. As a result of social distancing, infection peaks are lower and later than when a normal contact matrix is used.

Appendix A.3.4. Influence of social distancing on public space infection transmission

Contact matrices estimated by using the SFM were used to compare epidemiological curves between scenarios with and without social distancing, as shown in Figure 15. Public places where people can maintain social distancing are lessto becoming susceptible, exposed, infected, and then recovered from COVID-19 transmission.

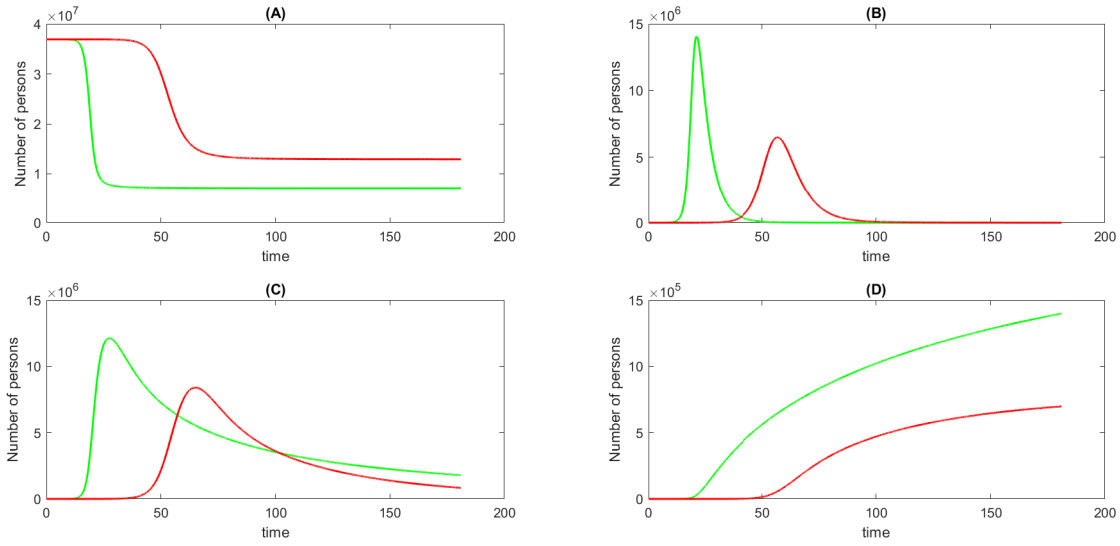

Figure 15. Normal contact matrix (green curve) versus social contact matrix (red curve) within public spaces. (A): evolution of susceptible individuals. (B): evolution of exposed individuals. (C): evolution of infectious individuals. (D): evolution of recovered individuals.

Appendix A.3.5. Cumulative number of infections and the reduction factor for normal contact and social distancing matrices

Table 4 presents the cumulative infections and reduction factors for normal contact matrices and social distancing matrices in various social contexts. Social distancing has been shown to lead to significant decreases in infections across all contexts, ranging from 40% in public spaces to 99% in workplaces.

Table 4. Cumulative infectious cases and their reduction factor for normal and social distancing contact matrices.

Places of activity	Households	Workplaces	Schools	Public spaces
Cumulative number of infectious for normal contact matrix	1.35×10^{11}	3.97×10^{10}	1.3×10^{11}	7.5×10^{10}
Cumulative number of infectious for social distancing contact matrix	2.83×10^{10}	5.74×10^{4}	2.1×10^{10}	4.5×10^{10}
Reduction (%)	80	99	83	40

Compared to other environments, workplaces displayed the largest reductions in infections (99%), which can be attributed to the frequent and prolonged contact between employees. By implementing social distancing measures, the number of contacts was reduced significantly and transmission risks were effectively mitigated. Among households, we observed the second-highest reduction (80%), demonstrating the importance of reducing intrafamily contact. There was a significant reduction (83%) in infections in schools by limiting inter-class contact, but the impact was less pronounced in public spaces, where there was a reduction of 40% in infections.

Appendix A.4. Results for infections dynamic comparison between social context survey-based contact matrices and our estimated SFM matrices

Here, we want to compare the infection dynamics in different social contexts for two sources of contact matrices: those derived from surveys and those estimated via the SFM. To simulate the epidemiological curves for each social context, we used the age-structured SEIR model and compared the results from an SFM-based contact matrix with a survey-based contact matrix.

Appendix A.4.1. Determining the infection dynamics in households by Using survey-based contact matrices and SFM-Based Contact Matrices

In Figure 16, the infectious individual peak based on SFM data (green curve) is slightly higher than that based on survey data (red curve). Given that the SFM-based contact matrix declines faster than the survey-based contact matrix after peak, there are near zero infectious individuals around day 170, while the survey-based contact matrix still shows a positive number until day 180.

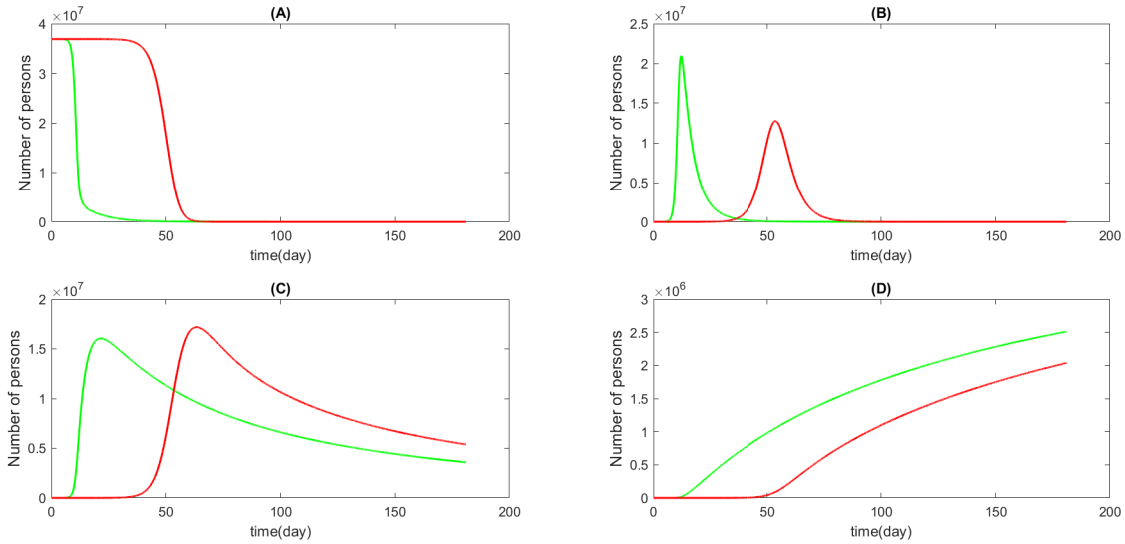

Figure 16. Normal contact matrix (green curve) versus survey-based contact matrix (red curve) results for within households. (A): evolution of susceptible individuals. (B): evolution of exposed individuals. (C): evolution of infectious individuals. (D): evolution of recovered individuals.

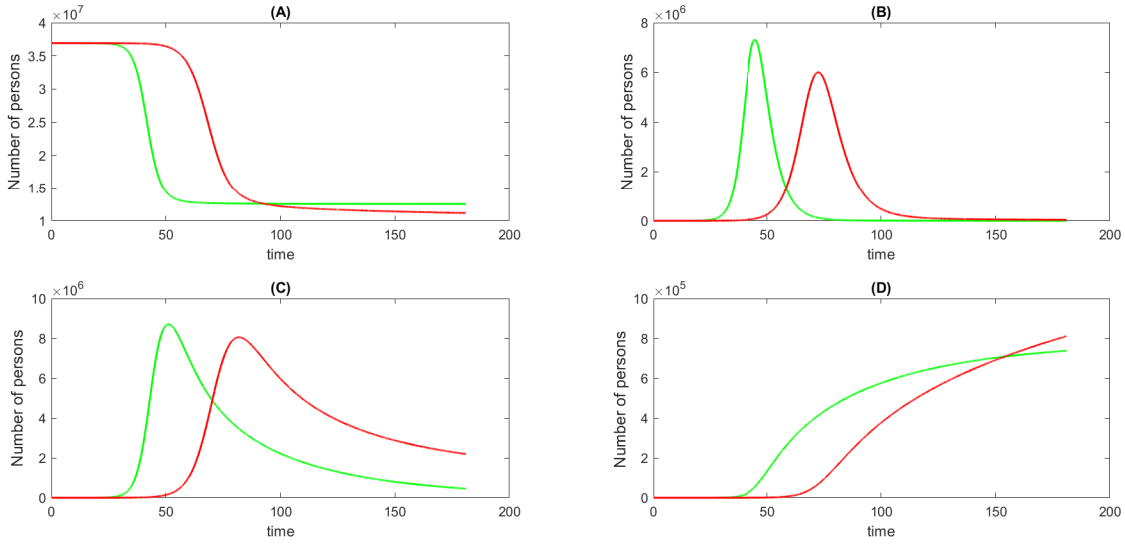

Figure 17. Normal contact matrix (green curve) versus survey-based contact matrix (red curve) results for within workplaces. (A): evolution of susceptible individuals. (B): evolution of exposed individuals. (C): evolution of infectious individuals. (D): evolution of recovered individuals.

Appendix A.4.2. Determining the infection dynamics in workplaces by using survey-based contact matrices and SFM-Based Contact Matrices

Figure 17 provides interesting insights regarding the comparison between the SFM-based contact matrices and survey-based contact matrices within workplaces.

First, both the SFM-based and survey-based contact matrices exhibit similar trends in the epidemiological curves, showing the evolution of susceptible, exposed, infectious, and recovered individuals. However, the SFM-based contact matrix (green curve) shows a higher peak and a faster spread of the infection than the survey-based contact matrix (red curve).

Appendix A.4.3. Determining the infection dynamics in other locations (public spaces and shopping centers) by using survey-based contact matrices and SFM-based contact matrices

Figure 18 presents a comparison of epidemiological curves for infection dynamics in public spaces for two sources of contact matrixes: SFM-based and survey-based.The results for infectious individuals due to the SFM-based contact matrix (green curve) are at a lower peak than those due to the survey-based contact matrix (red curve). Contact matrices from two sources differ based on the assumptions and methods used for their estimation, which may explain their differences. Unlike the survey-based Contact Matrix, which relies on self-reported data from questionnaires, the SFM-based contact matrix incorporates sociocultural factors such as interpersonal distances and desired walking speeds.

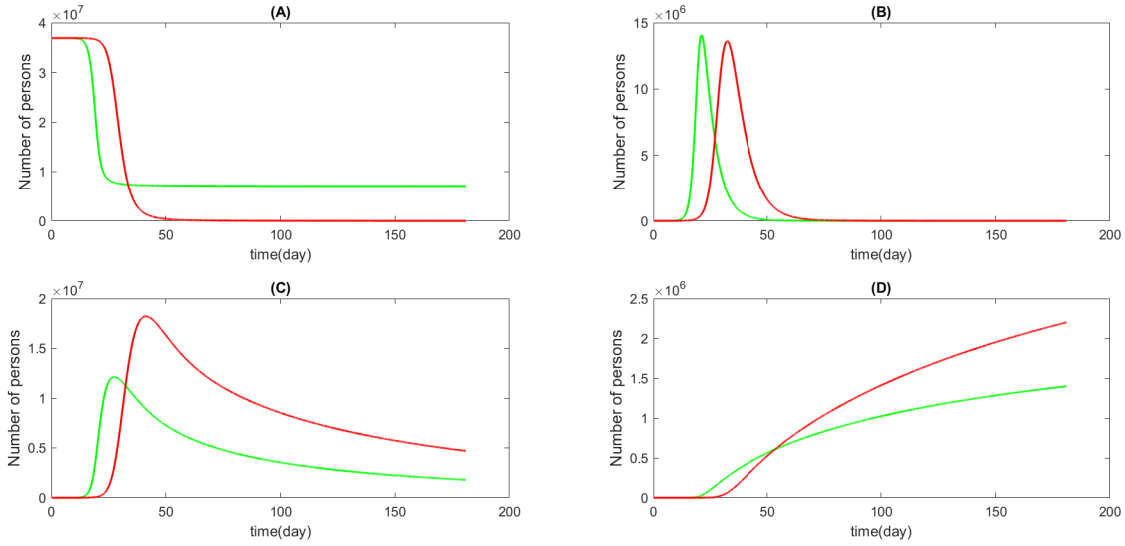

Figure 18. Normal contact matrix (green curve) versus Survey-Based contact matrix (red curve) results for within other locations. (A): evolution of susceptible individuals. (B): evolution of exposed individuals. (C): evolution of infectious individuals. (D): evolution of recovered individuals.

Appendix A.4.4. Cumulative infectious cases for normal SFM-based and survey-based contact matrices by activity location

Table 5 shows cumulative Infectious Cases with Normal and Survey-Based's Contact Matrices across Activity Locations. The results show that the SFM-based contact matrices produce lower estimates of the cumulative infectious cases than the survey-based contact matrices for all activity locations except households. As a result, SFM-based contact matrices capture social distancing-based matrix more accurately than survey-based contact matrices that assume homogeneity in compliance with distancing measures.

SFM-based contact matrices estimate about half as many infectious cases as survey-based contact matrices for other locations, where the difference between the two sources is particularly noticeable. The variation in interpersonal distances and contact frequencies among different age groups seems to be more sensitive to other locations.

In the cases of both sources, households account for the highest number of cumulative infectious cases. Interventions aimed at household contacts are necessary to control the spread of the epidemic. Workplaces and other locations are the leading sources of infection, followed by schools, which have the least effect on infection dynamics. In addition to the susceptibility and infectivity of different age groups, this reflects the age distribution and contact patterns at each activity location.

Table 5. Cumulative infectious cases for normal and survey-based contact matrices by activity location.

Places of activity	Households	Workplaces	Other locations
Cumulative number of infectious for normal contact matrix	1.35×10^{11}	3.97×10^{10}	7.5×10^{10}
Cumulative number of infectious for survey-based contact matrix	1.31×10^{11}	5.2×10^{10}	1.4×10^{11}

Appendix A.5. Classification of social distances

Here, we present the classification of social distances that we used to estimate the contact matrices for different social contexts. Given that it represents the physical space between two individuals, add their social distance can reflect their relationship and cultural norms. A study by Hall [17] distinguished four kinds of social distances: intimate, personal, social, and public. Each type of distance has its own range of values, as shown in Table 6. Based on the context and age group of agents, we determined the desired distances of agents in the SFM. In a household setting, for instance, agents prefer the intimate level of distancing, while in a shopping center, they prefer the social level of distancing. The desired distances [18] were varied to simulate different scenarios of social distancing and normal interactions.

Table 6. Types of social distances and their examples [17, 18].

Distance	Description	Example
0–0.4 m	Intimate distance	Parents, children, lovers, spouses, and partners
0.4–1.2 m	Personal distance	Close friends and family members
1.2–3 m	Social distance	Co-workers and acquaintances
3–4 m	Public distance	Strangers and officials

Appendix A.6. Population demographics within the place of activity

This section of the appendix contains data presented in Table 7 on the demographics of residents of different places of activity, including shopping centers, schools, homes, workplaces, and public spaces . Using the SFM, these data were used to estimate the contact matrices for each social context based on the sources cited in [14]. Based on the age distribution and frequency of Moroccans, the data show the percentage of each age group at each location. Social interactions in different settings are heterogeneous and variable, and these data help to capture these characteristics.

Table 7. Demography by age bracket for different locations. Information adapted from [14].

	Location				
Age bracket	Shopping centers	Schools	Households	Workplaces	Public Spaces
	Demography (%)	Demography (%)	Demography (%)	Demography (%)	Demography (%)
0-4	0	0.885	11.55	0	0
5-9	0.6	30.97	12.23	0	0.6
10-14	1	38.05	11.42	0	1
15-19	12.75	22.12	7.45	7.75	12.75
20-24	12.25	0.885	7.17	7.65	12.25
25-29	12.5	0.885	7.53	15.34	12.5
30-34	12.04	0.885	7.25	14.41	12.04
35-39	11.42	0.885	6.89	12.2	11.42
40-44	10.03	0.885	6.05	10.35	10.03
45-49	6.05	0.885	5.39	9.02	6.05
50-54	5.43	0.885	4.83	8.38	5.43
55-59	5.11	1.77	4.55	7.9	5.11
60-64	4.49	0	3.03	0	4.49
65-69	3.44	0	2.34	0	3.44
70-74	2.08	0	1.41	0	2.08
75-79	1.35	0	0.92	0	1.35

Use of AI tools declaration

The authors declare that they have not used artificial intelligence tools in the creation of this article.

Conflict of interest

The authors declare that there is no conflict of interest.

References

1. W. O. Kermack, A. G. McKendrick, A contribution to the mathematical theory of epidemics, *Proceedings of the Royal Society of London. Series A, Containing Papers of a Mathematical and Physical Character*, **115** (1927), 700–721. https://doi.org/10.1098/rspa.1927.0118
2. W. O. Kermack, A. G. McKendrick, Contributions to the Mathematical Theory of Epidemics–I. 1927, *Bull. Math. Biol.*, **53** (1991), 33–55. https://doi.org/10.1007/bf02464423
3. M. Y. Li, J. R. Graef, L. Wang, J. Karsai, Global Dynamics of a SEIR Model with Varying Total Population Size, *Math. Biosci.*, **160** (1999), 191–213. https://doi.org/10.1016/S0025-5564(99)00030-9
4. J. Mossong, N. Hens, M. Jit, P. Beutels, K. Auranen, R. Mikolajczyk, et al., Social Contacts and Mixing Patterns Relevant to the Spread of Infectious Diseases, *PLoS Med.*, **5** (2008), e74. https://doi.org/10.1371/journal.pmed.0050074
5. K. Prem, A. R. Cook, M. Jit, Projecting social contact matrices in 152 countries using contact surveys and demographic data, *PLOS Computat. Biol.*, **13** (2017), 1–21. https://doi.org/10.1371/journal.pcbi.1005697
6. K. Prem, K. van Zandvoort, P. Klepac, R. M. Eggo, N. G. Davies, Centre for the Mathematical Modelling of Infectious Diseases COVID-19 Working Group, et al., Projecting contact matrices in 177 geographical regions: an update and comparison with empirical data for the COVID-19 era, *PLoS Computat. Biol.*, **17** (2021), e1009098. https://doi.org/10.1371/journal.pcbi.1009098
7. A. C. E. Mouvoh, A. Bouchnita, A. Jebrane, A contact-structured SEIR model to assess the impact of lockdown measures on the spread of COVID-19 in Morocco's population, in *2020 IEEE 2nd International Conference on Electronics, Control, Optimization and Computer Science (ICECOCS)*, (2020), 1–4. 10.1109/ICECOCS50124.2020.9314462
8. R. Singh, R. Adhikari, Age-structured impact of social distancing on the COVID-19 epidemic in India, *arXiv preprint*, (2020), arXiv:200055. https://doi.org/10.48550/arXiv.2003.12055
9. Y. Xiao, M. Yang, Z. Zhu, H. Yang, L. Zhang, S. Ghader, Modeling indoor-level non-pharmaceutical interventions during the COVID-19 pandemic: A pedestrian dynamics-based microscopic simulation approach, *Transp. Policy*, **109** (2021), 12–23. https://doi.org/10.1016/j.tranpol.2021.05.004
10. D. Helbing, P. Molnar, Social Force Model for Pedestrian Dynamics, *Phys. Rev. E*, **51** (1995), 4282. https://doi.org/10.48550/arXiv.cond-mat/9805244
11. A. Jebrane, P. Argoul, A. Hakim, M. El Rhabi, Estimating Contact Forces and Pressure in a Dense Crowd: Microscopic and Macroscopic Models, *Appl. Math. Model.*, **74** (2019), 409–421. https://doi.org/10.1016/j.apm.2019.04.062
12. D. Helbing, I. J. Farkas, P. Molnar, T. Vicsek, Simulation of Pedestrian Crowds in Normal and Evacuation Situations, *Pedestrian and Evacuation Dyn.*, **21** (2002), 21–58.
13. D. S. I. Kanté, A. Jebrane, A. Hakim, A. Boukamel, Characterization of Superspreaders Movement in a Bidirectional Corridor Using a Social Force Model, *Front. Public Health*, **11** (2023), 1188732. https://doi.org/10.3389/fpubh.2023.1188732

14. D. S. I. Kanté, A. Jebrane, A. Bouchnita, A. Hakim, Estimating the Risk of Contracting COVID-19 in Different Settings Using a Multiscale Transmission Dynamics Model, *Mathematics*, **11** (2023), 254. https://doi.org/10.3390/math11010254

15. A. Bouchnita, A. Jebrane, A Hybrid Multi-Scale Model of COVID-19 Transmission Dynamics to Assess the Potential of Non-Pharmaceutical Interventions, *Chaos Solitons Fractals*, **138** (2020), 109941. https://doi.org/10.1016/j.chaos.2020.109941

16. A. Bouchnita, A. Jebrane, A Multi-Scale Model Quantifies the Impact of Limited Movement of the Population and Mandatory Wearing of Face Masks in Containing the COVID-19 Epidemic in Morocco, *Math. Model. Nat. Pheno.*, **15** (2020), 31. https://doi.org/10.1051/mmnp/2020016

17. E. T. Hall, *The hidden dimension*, New York: Anchor, 1966.

18. A. Sorokowska, P. Sorokowski, P. Hilpert, K. Cantarero, T. Frackowiak, K. Ahmadi, et al., Preferred Interpersonal Distances: A Global Comparison, *J. Cross-Cult. Psychol.*, **48** (2017), 577–592. https://doi.org/10.1177/0022022117698039

19. B. Kabalan, P. Argoul, A. Jebrane, G. Cumunel, S. Erlicher, A Crowd Movement Model for Pedestrian Flow Through Bottlenecks, *Ann. Solid and Struct. Mech.*, **8** (2016), 1–15. https://doi.org/10.1007/s12356-016-0044-3

20. P. Wang, Understanding Social-Force Model in Psychological Principles of Collective Behavior, *arXiv preprint*, (2016), arXiv:1605.05146. https://doi.org/10.48550/arXiv.1605.05146

21. G. Luebben, G. González-Parra, B. Cervantes, Study of optimal vaccination strategies for early COVID-19 pandemic using an age-structured mathematical model: A case study of the USA, *Math. Biosci. Eng.*, **20** (2023), 10828–10865. https://doi.org/10.3934/mbe.2023481

22. M. O'Driscoll, G. R. D. Santos, L. Wang, D. A. T. Cummings, A. S. Azman, J. Paireau, et al., Age-specific Mortality and Immunity Patterns of SARS-CoV-2, *Nature*, **590** (2021), 140–145. https://doi.org/10.1038/s41586-020-2918-0

23. *Morocco: WHO Coronavirus Disease (COVID-19) Dashboard With Vaccination Data*, World Health Organization, 2023. Available from: `https://covid19.who.int/region/emro/country/ma`

24. M. El Baldi, A. Laghrissi, Z. Marso, F. Z. Chellat, M. Berraho, N. Tachfouti, et al., Prevalence and associated factors of COVID-19 among Moroccan physicians: A cross-sectional study, *Plos One*, **17** (2022), e0277157. https://doi.org/10.1371/journal.pone.0277157

25. C. Zhan, Y. Zheng, L. Shao, G. Chen, H. Zhang, Modeling the Spread Dynamics of Multiple-Variant Coronavirus Disease Under Public Health Interventions: A General Framework, *Inf. Sci.*, **628** (2023), 469–487. https://doi.org/10.1016/j.ins.2023.02.001

26. *Institutional site of the High Commission for Planning of the Kingdom of Morocco (HCP)*, HCP, 2018. Available from: `https://www.hcp.ma/Projections-de-la-population-totale-du-Maroc-par-age-simple-et-sexe-2014-2050_a2209.html`.

27. *Statista, Morocco: Age structre from 2012 to 2021*. Available from: `https://www.statista.com/statistics/502768/age-structure-in-morocco`.

28. F. Hadrya, A. Soulaymani, F. El Hattimy, Space-time COVID-19 Monitoring in Morocco, *Pan Afr. Med. J.*, **35** (2020), Suppl 2. https://doi.org/10.11604%2Fpamj.supp.2020.35.2.23505

29. *Pyramides des âges pour le monde entier de 1950 à 2100*, Population Pyramid, 2014. Available from: https://www.populationpyramid.net/fr/maroc/2020/.

30. M. El Jai, M. Zhar, D. Ouazar, I. Akhrif, N. Saidou, Socio-economic Analysis of Short-term Trends of COVID-19: Modeling and Data Analytics, *BMC Public Health*, **22** (2022), 1633. https://doi.org/10.1186/s12889-022-13788-4

31. C. Cheng, D. Zhang, D. Dang, J. Geng, P. Zhu, M. Yuan, et al., The Incubation Period of COVID-19: A Global Meta-Analysis of 53 Studies and a Chinese Observation Study of 11,545 Patients, *Infect. Dis. Poverty*, **10** (2021), 1–13. https://doi.org/10.1186/s40249-021-00901-9

32. *Louvain Medical, L'épidémie de SARS-CoV-2 en Afrique Sub-Saharienne, questions, craintes et espoir*, 2020. Available from: https://www.louvainmedical.be/fr/article/lepidemie-de-sars-cov-2-en-afrique-sub-saharienne-questions-craintes-et-espoir.

33. D. S. I. Kante, A. Lamghari, A. Jebrane, A. Boukamel, A. Hakim, Estimating Social Contact Matrices Using a Modified Social Force Model and Socio-Cultural Data, *International Conference on Research in Applied Mathematics and Computer Science (ICRAMCS 2022)*.

34. J. Dolbeault, G. Turinici, Heterogeneous social interactions and the COVID-19 lockdown outcome in a multi-group SEIR model, *Math. Model. Nat. Pheno.*, **15** (2020), 36. https://doi.org/10.1051/mmnp/2020025

35. M. J. Pedersen, N. Favero, Social Distancing during the COVID-19 Pandemic: Who Are the Present and Future Noncompliers?, *Public Adm. Rev.*, **80** (2020), 805–814. https://doi.org/10.1111%2Fpuar.13240 .

36. L. H. Duczmal, A. C. L. Almeida, D. B. Duczmal, C. R. L. Alves, F. C. O. Magalhães, M. S. D. Lima, et al., Vertical social distancing policy is ineffective to contain the COVID-19 pandemic, *Cadernos de Saúde Pública*, **36** (2020), e00084420. https://doi.org/10.1590/0102-311x00084420

37. W. Lyra, J.-D. do Nascimento Jr, J. Belkhiria, L. de Almeida, P. P. M. Chrispim, I. de Andrade, COVID-19 pandemics modeling with modified determinist SEIR, social distancing, and age stratification. The effect of vertical confinement and release in Brazil, *Plos One*, **15** (2020), e0237627. https://doi.org/10.1371/journal.pone.0237627

38. K. A. Auger, S. S. Shah, T. Richardson, D. Hartley, M. Hall, A. Warniment, et al., Association between statewide school closure and COVID-19 incidence and mortality in the US, *Jama*, **324** (2020), 859–870. https://doi.org/10.1001/jama.2020.14348

39. Y. Bo, C. Guo, C. Lin, Y. Zeng, H. B. Li, Y. Zhang, et al., Effectiveness of non-pharmaceutical interventions on COVID-19 transmission in 190 countries from 23 January to 13 April 2020, *Int. J. Infect. Dis.*, **102** (2021), 247–253. https://doi.org/10.1016/j.ijid.2020.10.066

40. S. Lai, N. W. Ruktanonchai, L. Zhou, O. Prosper, W. Luo, J. R. Floyd, et al., Effect of Non-Pharmaceutical Interventions to Contain COVID-19 in China, *Nature*, **585** (2020), 410–413. https://doi.org/10.1038/s41586-020-2293-x

41. E. Bosina, U. Weidmann, Estimating Pedestrian Speed Using Aggregated Literature Data, *Physica A*, **468** (2017), 1–29. https://doi.org/10.1016/j.physa.2016.09.044

42. *Haut Commissariat du Plan, Les Cahiers du Plan N°43 - Mars/Avril 2013*, Available online: https://www.hcp.ma/Les-Cahiers-du-Plan-N-43-Mars-Avril-2013_a1248.html (accessed on November 2021).

43. N. Mellouki, *Vieillissement et Mode Alimentaire: Étude Anthropologique à Marrakech*, Université Cadi Ayyad, Marrakech, PhD thesis, 2007. Available from: http://wd.fmpm.uca.ma/biblio/theses/annee-htm/FT/2007/these45-07.pdf.

44. *Ministry of Health*, Available online: https://www.sante.gov.ma/Documents/2019/05/Rapport%20de%20l%20enqu%C3%AAte%20Stepwise.pdf (accessed on November 2021).

45. M. Loukid, P. Montero, Croissance des Enfants de la Ville de Marrakech (Maroc): Analyse Comparative Avec des Enfants Espagnols, *Bulletins et Mémoires de la Société d'Anthropologie de Paris*, **3** (1991), 211–224. https://doi.org/10.3406/bmsap.1991.1783

46. *Ministry of National Education, Preschool and Sports*, Available online: https://www.men.gov.ma/Ar/Documents/Recueil2012-13_v25032013.pdf (accessed on December 2021).

47. G. Shaw, A. M. Williams, *Tourism and Tourism Spaces*, Thousand Oaks, CA, USA: SAGE Publications, 2004.

48. *The World Bank*, Available online: https://data.worldbank.org/indicator/SE.SEC.ENRL.TC.ZS?locations=MA, (accessed on March 2022).

49. *The World Bank*, Available online: https://data.worldbank.org/indicator/SE.PRM.ENRL.TC.ZS?locations=MA, (accessed on March 2022).

50. *Trading Economics*, Available online: https://tradingeconomics.com/morocco/employment-rate, (accessed on February 2022).

51. *United Nations*, Available online: https://www.un.org/development/desa/pd/content/household-size-and-composition-around-world-2017-data-booklet, (accessed on February 2022).

52. V. Vuorinen, M. Aarnio, M. Alava, V. Alopaeus, N. Atanasova, M. Auvinen, et al, Modelling Aerosol Transport and Virus Exposure with Numerical Simulations in Relation to SARS-CoV-2 Transmission by Inhalation Indoors, *Saf. Sci.*, **130** (2020), 104866. https://doi.org/10.1016/j.ssci.2020.104866

53. *Statista*, "Education in Morocco", Statista, 2022. Available from: https://www.statista.com/topics/7523/education-in-morocco/#topicOverview.(accessed on December 25, 2023).

54. Frommer's, Available online: https://www.frommers.com/destinations/morocco/planning-a-trip (accessed on December 2022).

55. B. Gorbunov, Aerosol Particles Generated by Coughing and Sneezing of a SARS-CoV-2 (COVID-19) Host Travel Over 30 m Distance, *Aerosol Air Qual. Res.*, **21** (2021), 200468. https://doi.org/10.4209/aaqr.200468

56. *High Commission for Planning*, Available online: https://www.moroccoworldnews.com/2019/01/262899/moroccan-tv-reading-exercising-hcp (accessed on December 2022).

57. F. Iozzi, F. Trusiano, M. Chinazzi, F. C. Billari, E. Zagheni,S. Merler, et al., Little Italy: An Agent-Based Approach to the Estimation of Contact Patterns - Fitting Predicted Matrices to Serological Data, *PLoS Comput. Biol.*, **6** (2010), e1001021. https://doi.org/10.1371/journal.pcbi.1001021

58. *Time well spent*, The Wall Street Journal. Available from: `https://partners.wsj.com/icsc/shopping-for-the-truth/time-well-spent/article`.

59. Z. J. Madewell, Y. Yang, I. M. Longini, M. E. Halloran, N. E. Dean, Factors Associated with Household Transmission of SARS-CoV-2: An Updated Systematic Review and Meta-Analysis, *JAMA Netw. Open*, **4** (2021), e2122240. https://doi.org/10.1001/jamanetworkopen.2021.22240

60. *MoroccoPedia*, "Education in Morocco", in *Morocco Travel*, Available online: `https://www.moroccopedia.com/education-in-morocco/#:~:text=School%20hours%20in%20Morocco%20depend,2%20p.m%20until%206%20p.m.` (accessed on December 25, 2023).

61. *Ministry of National Education, Preschool & Sports*, "Aperçu sur le Système Educatif Marocain", Available online: `https://www.men.gov.ma/Documents/aper%C3%A7u-systemeducatif-marocain2004.pdf` (accessed on December 25, 2023).

62. *Ministry of National Education, Preschool & Sports*, "Education indicators", Available online: `https://www.men.gov.ma/Ar/Documents/INDIC-EDUCATION2020-21.pdf` (accessed on December 25, 2023).

63. *Morocco Mall*, Available online: `https://www.moroccomall.ma/horaires` (accessed on December 2022).

64. J. Stokes, A. J. Turner, L. Anselmi, M. Morciano, T. Hone, The Relative Effects of Non-Pharmaceutical Interventions on Wave One Covid-19 Mortality: Natural Experiment in 130 Countries, *BMC Public Health*, **22** (2022), 1113. https://doi.org/10.1186/s12889-022-13546-6

AIMS Press